





# Physical vulnerability of the coastal zone under wind farms influence of the cities of Pedra Grande and São Miguel do Gostoso/RN, Brazil

Vulnerabilidade física e ambiental da zona costeira sob a influência de parques eólicos nos municípios de Pedra Grande e São Miguel do Gostoso/RN, Brasil

Ivens Lorrán Clemente de Lacerda<sup>1</sup> , Venerando Eustáquio Amaro<sup>1</sup> , Maria de Fátima Alves de Matos<sup>1</sup> ,  
Ada Cristina Scudelari<sup>1</sup> 

## ABSTRACT

This study consists of determining the physical vulnerability of the region of São Miguel do Gostoso and Pedra Grande (in northeastern Brazil) before and after wind farm installation. To perform such an investigation, an analysis of the coastline vulnerability of the aforementioned area was conducted, considering changes occurred in the past 30 years and spatially presented separately. The Natural Vulnerability Index (NVI) and Environmental Vulnerability Index (EVI) were calculated through analysis using thematic maps of geomorphology, geology, soils, vegetation, and land use and occupation variables, with their dimensionality and subjectivity determined by the execution of the hierarchical analytical process (HAP) and principal component analysis (PCA). High and very high vulnerability together showed proportions between 18 and 30% in all NVI and EVI scenarios. The Coastal Vulnerability Index (CVI) was defined using two methodologies for the three scenarios of sea level rise established by the Intergovernmental Panel on Climate Change (IPCC): the first one includes six physical or hydrodynamic variables, and the second includes, beyond these, three more variables of anthropogenic action. In all of the applied scenarios, the medium and high vulnerabilities dominated all along the coastline, with the second method being the most optimistic. We can conclude that the installation of the wind farm complex contributed to the increase of the vulnerability of the local ecosystems regarding the three investigated indices; however, it was not the preponderant factor for the determination of the CVI vulnerability degree.

**Keywords:** multitemporal analysis; coastal erosion; environmental vulnerability index; natural vulnerability index.

## RESUMO

Este estudo visa à determinação da vulnerabilidade física e ambiental da zona costeira de São Miguel do Gostoso e Pedra Grande/RN antes e depois da instalação de parques eólicos. Além disso, é realizada uma análise de vulnerabilidade na linha de costa da área mencionada, levando-se em consideração as alterações espaciais concretizadas nos últimos 30 anos, análise esta que é apresentada separadamente. Calcularam-se os índices de vulnerabilidade natural (IVN) e ambiental (IVA) por meio de análises espaciais baseadas em mapas temáticos das variáveis do meio físico e antrópico, conforme métodos de análise multicritérios hierarquizada e de redução de dimensionalidade por processo analítico hierárquico (PAH) e pela análise de componentes principais (ACP). As vulnerabilidades alta e muito alta, somadas, apresentaram proporções entre 18 e 30% em todos os cenários do IVN e IVA. O índice de vulnerabilidade costeira (IVC) foi definido por dois métodos para três cenários de aumento do nível do mar estabelecidos pelo Painel Intergovernamental de Mudanças Climáticas (IPCC): um com seis variáveis físicas e hidrodinâmicas, e outro que inclui, além destas, outras três variáveis de ação antrópica. Para todos os cenários, toda a extensão da linha de costa mostrou-se, majoritariamente, com vulnerabilidades média e alta. Conclui-se que a implantação do complexo de parques eólicos contribuiu para o aumento da vulnerabilidade dos ecossistemas locais nos três índices avaliados, mas não foi o fator preponderante para a definição do grau de vulnerabilidade do IVC.

**Palavras-chave:** análise multitemporal; erosão costeira; índice de vulnerabilidade ambiental; índice de vulnerabilidade natural.

<sup>1</sup>Universidade Federal do Rio Grande do Norte – Natal (RN), Brazil.

Correspondence address: Ivens Lorrán Clemente de Lacerda – Rua Aprígio Veloso, 175, apto. 306 – Bairro Universitário – CEP: 58429-170 – Campina Grande (PB), Brazil.

E-mail: ivenslorran@hotmail.com

Conflicts of interest: the authors declare that there are no conflicts of interest.

Funding: Coordenação de Aperfeiçoamento de Pessoal de Nível Superior Brasil (CAPES); Universidade Federal do Rio Grande do Norte (UFRN).

Received on: 10/10/2021. Accepted on: 07/01/2022

<https://doi.org/10.5327/Z2176-94781244>



This is an open access article distributed under the terms of the Creative Commons license.

## Introduction

Erosive processes result from frequent phenomena that transform the soil and alter the dynamics and distribution of sediments along the coast. Coastal zones are among the most affected regions by these processes (Silva et al., 2020), and in recent years, greater climate variability and global environmental changes have intensified erosion in these sectors due to the relative rise in the mean sea level (MSL) (Martínez et al., 2018). In addition to this, changes in land use and cover, as well as the construction of infrastructures in areas close to the seafloor, interfere with the sedimentary balance of the entire adjacent coastal zone, leaving it more susceptible to erosion processes and changes in the environment, which result in the advance of the coastline (henceforth CL) toward inhabited areas (Menezes et al., 2018).

According to a series of measurements by tide gauges since 1946, complemented by satellite altimeters, the MSL rises at an average rate of 3.6 mm/year along the Brazilian coast (Short and Klein, 2016), which highlights its estimated increase of approximately 0.43 m in an optimistic scenario and approximately 0.84 m in a pessimistic scenario by the year 2100 according to the Intergovernmental Panel on Climate Change forecast (IPCC, 2019). Hinkel et al. (2013) estimated that coastal zones will lose between 6,000 and 17,000 km<sup>2</sup> of area, forcing the displacement of around 5.3 million people.

The coastal zone of the State of Rio Grande do Norte (RN) has stood out in the production of wind energy due to the continuous action of the trade winds, which makes it the largest producer of this type of energy in Brazil (Rodrigues et al., 2017). The production of wind energy in the coastal marine biome, which is environmentally sensitive, exposes negative aspects related to the changes imposed on biotic, physical, and anthropogenic environments, from the implementation stages to the operation of wind turbines and other associated infrastructures. Among the impacts caused by the continuous action of wind turbines, the following impacts stand out: scenic interference, vegetation suppression, natural soil removal and/or addition of allochthonous soil, interference in the health of the surrounding population, noise emission, species extinction, stroboscopic effect, land lease, reduced agricultural production, and stress on the behavior of local fauna, whether marine or terrestrial (Nazir et al., 2019; Nogueira et al., 2020).

In addition to these impacts, the sectors known for having the greatest potential for wind energy generation in Brazil, that is, with greater constancy and annual average wind speeds, are permanent protection areas (PPAs), legally protected by the Forest Code Law No. 12651/2012 (Brasil, 2012) and by CONAMA's Resolution No. 303/2002 (Brasil, 2002). PPAs are preserved or recovering areas whose main function is the maintenance or conservation of ecosystems and natural resources. In coastal zones, such laws determine that restingas, mangroves, and the 100 m horizontal strip from the edge of plateaus or tablelands have guaranteed preservation. Dunes, in turn, are highlighted as PPAs only in the second of the aforementioned guidelines, commonly generating legal differences in decisions involving environmental licensing (Vieira, 2019).

Anthropogenic occupation and industrial uses of natural resources commonly accelerate environmental changes as a result of local re-

modeling required by construction processes for infrastructure installations. Such changes can potentially promote negative and irreversible impacts on coastal ecosystems, forcing detailed studies that, in addition to local contextual updating, list geoenvironmental factors based on multitemporal analyses and future scenario projection in order to combine sustainability criteria and economic interests, especially industrial ones related to renewable energy (IPCC, 2021).

The concept of vulnerability addressed by the AR5-IPCC (IPCC, 2014) is adopted in most research involving the physical vulnerability of territory units and is defined as the predisposition of a space to be adversely affected, involving other concepts and elements, such as susceptibility to damage and lack of support and adaptation.

The definition of physical vulnerability involving spatial analyses and prognosis is well accepted and widespread in research carried out in all parts of the world (Gornitz et al., 1994; Crepani et al., 2001; Busman et al., 2016; Gerrity et al., 2018). This assessment is performed using indices such as the natural vulnerability index (NVI), the environmental vulnerability index (EVI), and the coastal vulnerability index (CVI). The NVI is obtained from the intersection of geoenvironmental factor properties based on the ecodynamic principles of Tricart (1977) and was introduced by Crepani et al. (2001). Grigio et al. (2004) adapted this index and proposed the EVI, which is defined as the susceptibility of an area to suffer damage considering anthropogenic or human action.

The CVI identifies coastal areas affected by the MSL increase, considering other physical variables such as geology, geomorphology, slope angle, and local variations of the CL and hydrodynamic variables such as significant wave height, tidal range, and relative MSL increase historically. This index was initially proposed by Gornitz et al. (1994), and among the various adaptations to this methodology found in the literature, that of Busman (2016) stands out for incorporating variables such as coastal urban infrastructure, established activities or uses, and the prognosis of CL variation into the equation. Therefore, the CVI highlights the changes caused by natural factors, often influenced by human activities that found in the CL, and assumes the CL retreat toward the continent or CL retraction (Pantusa et al., 2018).

Accordingly, different pieces of research adjust these indices to local specificities, and in Brazil, a few studies stand out, such as those proposed by Menezes et al. (2018) on the coast of Pernambuco, Luz et al. (2019) on the riverside region of Mato Grosso, and Amaro et al. (2021a) on the coast Rio Grande do Norte, since they integrate vulnerability to erosion into their studies with the help of geoprocessing techniques, and are located in regions similar to the one in our study. Gerrity et al. (2018) in the United States, Koroglu et al. (2019) in Spain, and Pantusa et al. (2018) in Italy apply the CVI, while Choudhary et al. (2018) in Russia and Liu et al. (2017) in China employ EVI and NVI, which endorse the body of research on physical vulnerability.

The main objective of this study was to determine the physical and environmental vulnerability of the coastal region of Pedra Grande and São Miguel do Gostoso in the State of Rio Grande do Norte before and after the

installation of the União dos Ventos Wind Farm Complex and to verify the hypothesis of increased vulnerability with the introduction of wind turbines through the characterization of geoenvironmental units such as geology, geomorphology, pedology, vegetation, and land use and cover and the determination of environmental, natural, and coastal vulnerability indices.

### Characterization of the study area

The study area is located on the northern coast of the State of Rio Grande do Norte, northeastern Brazil, between the cities of Pedra Grande and São Miguel do Gostoso (Figure 1). It has an area of approximately 111 km<sup>2</sup> with 19 km of CL extension and an average of 5.9 km in length toward the mainland, in a territory known for its tourist relevance, where the União dos Ventos Wind Complex is located, composed of 137 wind turbines installed in 2012 and capable of producing 235 MW of electricity (ANEEL, 2020).

This region is located in the tropical coastal semi-arid subdomain of the Eastern Brazilian Northeast. The convergence of northeast (NE) and southeast (SE) trade winds transports moisture over this equatorial region. Their mean monthly speed varies from 6.53 to 8.89 m/s in dry months, and from 5.85 to 8.39 m/s in the rainy season (EC-MWF, 2020). The Calcanhar Meteorological Station (code A344), the one closest to the study area, indicated a mean annual temperature of 26.6°C and an average annual rainfall of 1,035.88 mm in the rainy season, from March to July, in the period from 2008 to 2018 (INMET, 2020). Its regime is that of semidiurnal mesotides with a mean level of 139 cm above the reduction level, with mean high tides of syzygy of 234 cm, mean quadrature high tides of 221 cm, mean low tides of syzygy of 43 cm below RN, and mean quadrature low tides of 56 cm (Matos et al., 2011). The wave direction is predominantly NE with an average period of 6.0 s and a significant height of 0.9 m, sometimes reaching the periods of 8 s and 2.2 m of significant height (Matos et al., 2017).

The area of interest includes the geological context of the Potiguar Basin, with a predominance of coastal beach deposits and mobile and fixed dunes, which are notably interconnected. They are composed of fine- to coarse-grained quartz sand, which is whitish in color and covers other geological units throughout the region (Diniz Filho et al., 2018).

The geomorphology is marked by flat-topped coastal tablelands, predominantly Barreiras Formation lithology, with heights varying between 10 and 50 m, markedly evident in the active cliffs (Macedo et al., 2017). The equally flat and low coastal plain, with elevations of less than 10 m, is dominated by sandy beaches connected with the fields of mobile and fixed dunes.

Vegetation cover varies from hypoxerophytic shrub-arboreal caatinga in coastal plateau sectors to herbaceous grass on the beach strip working as a dune stabilizer (Macedo et al., 2017). In the vicinity of water courses, floodplain fields can be observed. The local pedology is dominated by Hydromorphic Quartzarenic Neosol, Quartzarenic Neosol, and Chromic Luvisol (Embrapa, 2018).

### Methodology

#### Physical vulnerability indices

The construction of physical vulnerability indices was based on the methodologies described by Gornitz (1991), Crepani et al. (2001), Grigio et al. (2004), and Busman (2016) using, as primary information, the maps of geoenvironmental factors (geology, geomorphology, pedology, and vegetation), land use and cover, and physical and hydrodynamic data of the coastal area. The natural and environmental vulnerability indices determined for the coastal zone were treated and spatially presented separately from the CVI, responsible for analyzing only the coastline of the same region. All the maps, with a scale of 1:100,000, were generated in a Geographic Information System (GIS) environment through the analysis and interpretation of images from the LANDSAT 5 satellites of the Thematic Mapper (TM) sensor of July 8, 2009, with a spatial resolution of 30 m for the visible to the infrared bands (bands 1–5 and 7), and LANDSAT 8 images from the Operational Land Imager (OLI) sensor of October 8, 2019, with a spatial resolution of 30 m for the visible to the infrared bands (bands 1 to 9), and 15 m for the panchromatic band (band 8), both from scene 215/064. The Digital Elevation Models (DEMs) and slope angle were prepared based on images from the Shuttle Radar Topography Mission (SRTM) with a spatial resolution of 30 m.

#### Preparation of thematic maps

The spectral enhancement of the images in this study was obtained by manipulating the images using Digital Image Processing techniques on the ER Mapper 7.1 software. Georeferencing for the correction of distortions in geopositioning used the geodetic reference Geocentric Reference System for the Americas (SIRGAS2000) and the Universal Transverse Mercator (UTM) cartographic projection in zone 25S, reaching the mean-squared error (MSE) of less than 1.0.

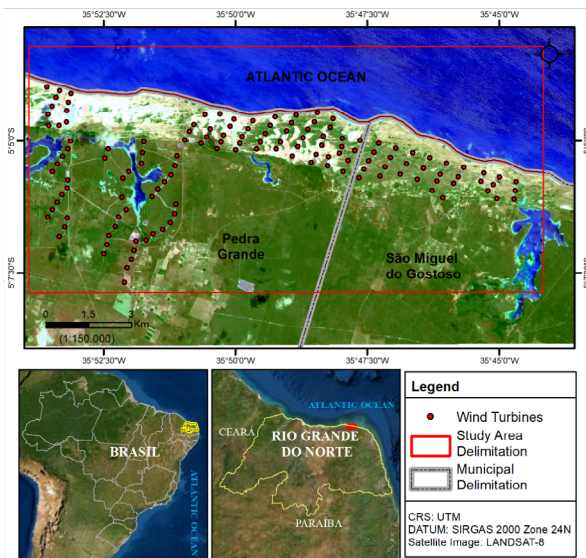


**Figure 1 – Study area located in the cities of Pedra Grande and São Miguel do Gostoso, on the northern coast of the State of Rio Grande do Norte.**

To enhance the thematic features through multispectral bands, color composition was applied using the red-green-blue (RGB) system and the red-green-blue-intensity (RGBI) hybrid system, including the Normalized Difference Vegetation Index (NDVI) in order to highlight the specific thematic features for the analysis and visual interpretation, as well as in the creation of thematic maps in GIS. The selection among the multispectral bands considered the spectral signatures of the units present on the surface (Pereira et al., 2011; Loebmann et al., 2012). The images in the hybrid RGBI system incorporate a panchromat-

ic image, increasing the gain to a spatial resolution of 15 m (Pereira et al., 2011). The supervised classification technique was employed in the drawing of the land use and cover maps through the maximum likelihood method.

In the ArcMap 10.3 GIS environment, thematic maps were prepared for the years 2009 and 2019 based on the visual interpretation of the multispectral colored images for the variables such as geology (Figure 2A), geomorphology (Figure 2B), pedology (Figure 2C), vegetation (Figure 2D), and land use and cover (Figure 2E).

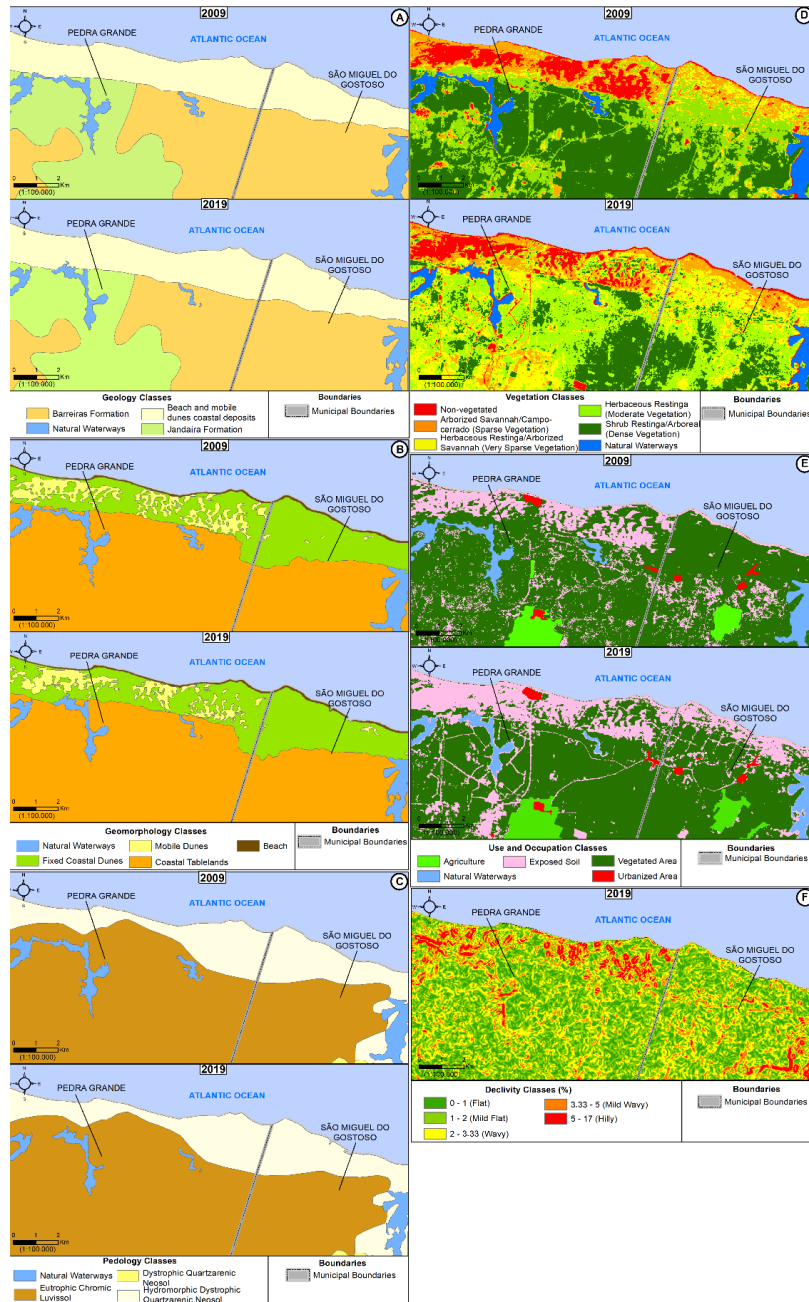


Figure 2 – Thematic maps of the study area (in the terrestrial environment) for the years 2009 and 2019: (A) geology, (B) geomorphology, (C) pedology, (D) vegetation, and (E) use and occupation. (F) Slope map for the year 2019.

In addition to the information obtained through satellite images, the thematic maps were made with the aid of past maps from the Mineral Resources Research Company (CPRM), for the variables geology, geomorphology, and pedology; and the Brazilian Institute of Geography and Statistics (IBGE) and the Brazilian Agricultural Research Corporation (Embrapa) in the slope and pedology maps. The DEM and the slope map (Figure 2F), drawn only for the year 2019, were based on the SRTM and geodetic survey support with points from the Geodetic Network of the Northern Coast of RN (Santos and Amaro, 2011).

#### Natural and environmental vulnerability indices

The NVI and EVI represent the susceptibility of thematic variables (geology, geomorphology, pedology, vegetation, and use and occupation) to temporal variations, such as erosion, in the study area. The EVI differs from IVN due to the insertion of the variable use and occupation, necessary to identify the changes generated in the region resulting from human activities, including the installation of the wind farm. Initially, the vulnerability was assessed for each class of these variables for the years 2009 and 2019.

For this, scores were established for all the classes of each variable with an interval of 0.5 on a scale ranging from 1 to 5, with 1 for very stable and less vulnerable areas and 5 for very unstable and vulnerable ones. The scores established for each class were based on the work of Crepani et al. (2001), Grigio et al. (2004), Busman et al. (2016), and Amaro et al. (2021b), most of which were carried out in similar coastal geographic conditions in other regions of RN (Table 1).

The natural vulnerability map is the result of the intersection of vulnerability maps for thematic variables (geology, geomorphology, vegetation, and soil) with the scores assigned to each class, following an equation that involves all variables. Saaty's (2008) weights were used, generating weights for each variable through the analytical process of hierarchy (APH). After obtaining the weights, the NVI and the EVI were calculated using ArcMap 10.3 by the sum of the variables multiplied by their respective weighting (Equations 1 and 2). The results were then classified by the degree of vulnerability following the Boolean logic (Table 2) according to Crepani et al. (2001).

$$NVI = 0,077 \times GEO + 0,501 \times GEOM + 0,159 \times SOL + 0,263 \times VEG \quad (1)$$

$$EVI = 0,064 \times GEO + 0,355 \times GEOM + 0,112 \times SOL + 0,211 \times VEG + 0,258 \times USO \quad (2)$$

Where:

NVI = natural vulnerability index;

EVI = environmental vulnerability index;

GEOM = geomorphology;

GEO = geology;

VEG = vegetation;

SUN = soil;

USE = land use and cover.

**Table 1 – Scores for each class for determining vulnerability indices following Boolean logic.**

Variable	Class	Scores
Geology	Coastal beach deposits and mobile dunes	5
	Barreiras Formation	2.5
	Jandaíra Formation	1.5
Geomorphology	Fixed dunes	3.5
	Mobile dunes	5
	Beach	5
	Coastal plateau	1.5
Pedology	Eutrophic chromic luvisol	3
	Dystrophic Quartzarenic Neosol	4
	Dystrophic Hydromorphic Quartzarenic Neosol	5
Vegetation	Absence of vegetation	1
	Wooded Savanna/Campo-cerrado	3
	Restinga Herbácea/Wooded Savanna	4
	Herbaceous restinga	4
	Shrub restinga/Arboreal	3
Use and cover	Agriculture	3
	Urbanized area	5
	Vegetated area	2
	Exposed soil	4

**Table 2 – Ranges of vulnerability classes following Boolean logic.**

Very low	Low	Medium	High	Very high
1–1.8	1.8–2.6	2.6–3.4	3.4–4.2	4.2–5

In the NVI and EVI equations, geomorphology had greater weight due to its strong ability to change in the face of severe weather. The geology and pedology variables do not undergo so many changes on this time scale and receive the lowest weights. Intermediate weight was assigned to the vegetation variable due to the role it plays in controlling erosion and runoff. Intermediate values were also attributed to the variable land use and cover since anthropogenic action significantly and quickly interferes in the physical dynamics of the territory.

#### Coastal vulnerability index

In this research, the CVI was calculated by the following two methodologies: CVI-USGS proposed by Gornitz et al. (1994), and CVI proposed by Busman (2016). The quantification of the CL variation was used as a reference for the erosion/accretion rate extracted from the analysis of the dry/wet line (Amaro et al., 2015) from the LANDSAT 5 TM and LANDSAT 8 OLI satellite images of August 2, 1989, July 29,

1999, July 8, 2009, and October 8, 2019, under similar high tide conditions, varying between 0.29 m and 0.61 m. Erosion/accretion rates were determined by linear least square regression (linear regression [LRR]). The CL variation prognosis was performed using the least median square (LMR) in the CL.

The local tide data were obtained through the method proposed by Formigoni and Araújo (2015) based on the interpolation of tidal range values from the tide tables provided by the Directorate of Hydrography and Navigation (DHN, 2020) of the Brazilian NAVY, from the ports of Natal and Macau. The significant wave height data in the CL of the study area were acquired through the analysis of the historical series of data between 1979 and 2019 in ERA5 developed by the European Center for Medium-Range Weather Forecasts.

The MSL variation parameter was based on three of the four scenarios called Representative Concentration Pathway (RCP), adopted by the IPCC in their Fifth Climate Change Report (IPCC, 2014): optimistic scenario (RCP 2.6, with low concentrations), intermediate scenario (RCP 4.5, with moderate concentrations), and pessimistic scenario (RCP 8.5, with high concentrations). The CVI was also classified according to vulnerability in five categories, ranging from very low to very high (Table 3). The categorization was supported by the works of Gornitz (1991), Busman (2016), and Amaro et al. (2021b).

In the NVI and EVI, there was some discrepancy between the importance of the variables used to determine the indices, as previously justified. In the CVI, it was not deemed necessary to differentiate the relevance between the factors listed, whether physical or hydrodynamic ones. Therefore, in this study, we chose to calculate the two indices through arithmetic mean, reproducing the methodological proposal by Busman (2016) according to the Equations 3 and 4:

$$CVI - USGS = \frac{(GEOM + CLV + DEC + SWH + AMP + SCEN)}{6} \quad (3)$$

$$CVI = \frac{(GEOM + CLV + DEC + SWH + AMP + SCEN + CLVPROJ + INFRA + USE)}{9} \quad (4)$$

Where:

CVI = coastal vulnerability index;

GEOM = geomorphology;

CLV = coastline variation;

DEC = slope;

SWH = significant wave height;

AMP = tidal amplitude;

SCEN = relative mean sea level rise scenarios;

CLVPROG = prognosis of coastline variation;

INFRA = urban infrastructure;

USE = type of use or activity.

**Table 3 – Valuation of the classes of variables to determine the indices of coastal vulnerability following Boolean logic.**

Variable	Class	Degree
Slope (shoreline and emerged portion of the beach)	> 5%	Very low
	3.33–5%	Low
	2–3.33%	Medium
	1–2%	High
	0–1%	Very high
Geomorphology	Fixed dunes	Very low
	Mobile dunes	High
	Beach strip	Very high
Coastline variation rate	-2 to 2 m/year	Medium
	-2 to -10 m/year	High
Significant wave height	1.48 m	Very high
Tidal range	0.91 m	Very low
Mean sea level variation	RCP 2.6	Medium
	RCP 4.5	High
	RCP 8.5	Very high
Use/activity	Vegetated Area	Very low
	Exposed Soil	Low
	Urbanized Area	Very high
Urban infrastructure	Absent	Very low
	Leisure; Coastal Eng.	Very high
Projection of coastline variation	-2 to 2 m/year	Medium
	-2 to -10 m/year	High

## Results and Discussion

The results of the attribution of scores to each class of geo-environmental factors showed the classification regarding the degree of vulnerability of the coastal zone (Figure 3) for the years 2009 and 2019. The results indicate negligible changes in proportions in the classes of geomorphology, geology, and pedology, while the land use and cover variables, especially vegetation, undergo significant changes. Human actions influence the land use and land cover classes as well as vegetation, especially through deforestation and burning to prepare the soil for planting/pasture, and various uses with activities of some degree of urbanization and wind farm installation.

The local geomorphology maps (Figure 2B) show that the wind turbines were installed, mostly, under mobile dune fields. Only part of the wind turbines are located under the coastal plateau terrain, with only one of them located close to the morphological rupture line on the CL, the active cliffs. The dune fields and the horizontal strip 100 m

from the edges of the coastal plateau are considered PPAs by CONAMA's Resolution No. 303/2002. Therefore, the emergence of large enterprises in these areas can cause serious geoenvironmental and social problems for ecosystems and local communities. Since these are regions with high coastal dynamics, any type of use and occupation of this territory must be carefully evaluated before granting licenses for human intervention in order to avoid increased vulnerability and the definitive destruction of ecosystems.

The implementation of the wind farm complex has changed the thematic variable of land use and cover since large areas were modified for the installation of wind turbines and for the creation of access roads for the wind turbines and other facilities in the complex, which was verified in the increase in the high vulnerability class when comparing the years 2009 and 2019. The layout of access roads and infrastructure, together with the agricultural expansion, suppressed original vegetation cover, which made this variable experience changes proven by the advancement of the high vulnerability class, which increased by approximately 10% from 2009 to 2019.

To validate the weights adopted for the NVI and EVI equations, we carried out a statistical analysis that is responsible for the evaluation of the most important variables in a system, i.e., principal component analysis (PCA). This methodology was applied to the area proportions of each vulnerability class of the NVI and EVI maps for the years 2009 and 2019. For both cases, the accumulated variance of the first three principal components was greater than 95%, indicating acceptable representativeness of the results. In the NVI, the weights of the variables indicated that pedology was the most important one, obtaining a strong degree of correlation in PC1, with a weight modulus greater than 0.75 according to Pearson's intervals (Colton, 1974). PC2 and PC3 were marked by the geology and geomorphology variables and the vegetation variable, respectively, all with a moderate degree. In the EVI, pedology continued to be the predominant variable, but this time together with use and cover, both with a moderate degree of correlation. The geomorphology variables appeared with moderate correlation and the vegetation with strong correlation, which compose PC2 and PC3, respectively.

In the NVI and EVI equations, geomorphology had greater weight due to its strong capability to change in the face of severe weather. The geology and pedology variables do not undergo so many changes on this time scale, receiving the lowest weights. Intermediate weight was assigned to the vegetation variable due to the role it plays in controlling erosion and runoff. Intermediate values were also attributed to the variable of use and cover, since human action significantly and quickly interferes in the physical dynamics of the territory. The results found for the NVI showed significant differences in the investigated period (Figure 4A).

The class with very high vulnerability corresponds predominantly to the coastal strip, with 1.31% of the total area in 2009 and 0.80% in 2019. Vegetated or mobile dune fields composed the high vulnerability class between 2009 and 2019, with values of 23.47% and 24.69%, respectively. The medium and low vulnerability classes were distributed around the totality of the coastal plateaus, having the values of 15.51 and 55.85% in 2009, respectively, and of 23.04 and 47.71% in 2019, respectively. The very low vulnerability class indicated the values of 0.77 and 1.23% in 2009 and 2019, respectively.

The EVI results indicated similarities in the degrees of vulnerability for the investigated years (Figure 4B). The very high vulnerability class, with 1.10% of the total area in 2009 and 0.93% in 2019, corresponds to the coastal strip. High vulnerability marked the sectors of mobile dune fields with the values of 15.94 and 21.80% in 2009 and 2019, respectively, indicating a significant increase in environmental vulnerability. The medium vulnerability class showed the values of 27.28 and 18.14% in 2009 and 2019, respectively, which were present mainly in the coastal plateaus with exposed soil and in vegetated dunes. Low and very low vulnerability classes occurred in the vegetated coastal plateau, the former being the most representative, with 54.85 and 0.84% in 2009, respectively, and 58.76 and 0.38% in 2019, respectively.

Figure 5 summarizes that among the four area proportion graphs of the weighted indices, low, medium, and high vulnerabilities together add up to more than 95% of the total area for all indices in all years. The low vulnerability stands out since it represents most of the area in the investigated period of both indices, especially by its occurrence in coastal plateau sectors.

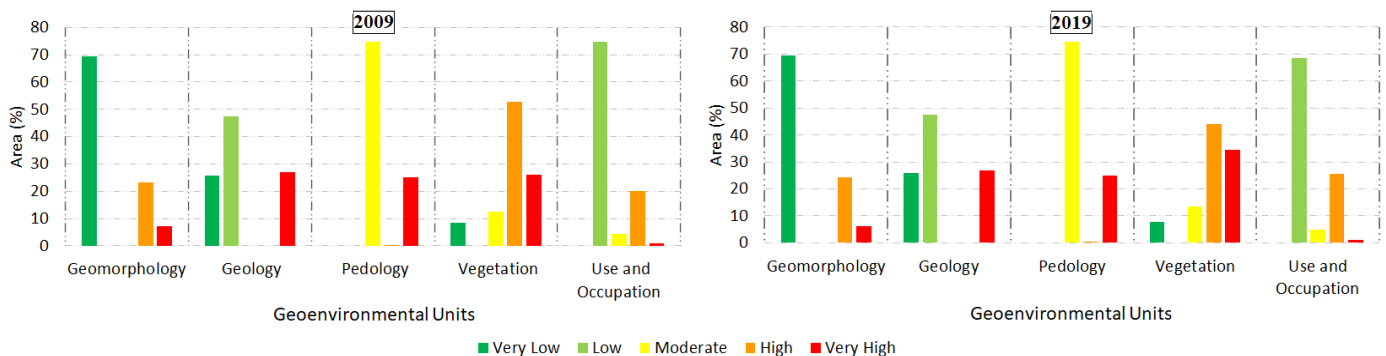


Figure 3 – Proportion of areas affected by each degree of vulnerability displayed for each variable individually in the years: (A) 2009 and (B) 2019.

In the NVI, there was an increase in the medium vulnerability and, consequently, a reduction in the low vulnerability class, while the high vulnerability indicated a slight increase between the 2 years. In terms of EVI, there is an increase in the classes of high and low vulnerability, which implies a significant decrease in the proportion of sectors with a medium vulnerability class. In both indices, the very high vulnerability class defines the sectors of the coastal strip with a predominance of the physical aspects of the thematic variables, such as geology and pedology, and, above all, in terms of geomorphological criteria, variables proved to be the most influential in this research. The addition of the use and cover variable to the equation caused the increase of high and very high vulnerability classes in the total context of the study area, but mainly in the sectors defined by the dune fields, which confirms the aforementioned influence of the installation of wind turbines.

The CL variation, analyzed through DSAS 4.4, for the years 1989, 1999, 2009, and 2019 through the Net Shoreline Movement (NSM) method indicated the amplitudes of variations of 114.64 m, with a minimum value of -103.76 m and a maximum value of approximately 10.88 m. Therefore, the sedimentary dynamics in the evaluated stretch indicated the predominance of coastal erosion in general. Statistical data referring to this variation are summarized in Table 4.

The LRR and LMS methods indicated negative values for the mean, median, mode, and total sum, and very low maximum values compared

to the minimum values. This fact indicates the continuous retraction of CL in the investigated period of the last 30 years, a trend which, if maintained, will also extend the current issues to the next decades. In other words, in the local sedimentary dynamics, erosion processes are dominant and intense, as indicated by the LRR and the LMS, which represent, respectively, the accretion/erosion rate and the projection of this rate.

With the incorporation of the urban infrastructure, projection of the CL variation, and land use classes, the CVI (Busman et al., 2016) resulted in a CL subdivided into the dominant classes between medium and high vulnerabilities, increasing the stretches with high vulnerability for the scenarios with MSL variation, with RCP 4.5 and RCP 8.5 (Figures 6A and 6B).

In this method, there is a greater similarity in the same CL sections in the three projections. In the city of Pedra Grande, the turbines located in the vicinity of the CL, installed at distances ranging from 101 to 171 m from the maximum high tide line, are located in sectors considered to be of high vulnerability in both methods and for any of the scenarios with MSL increase. In the section corresponding to the city of São Miguel do Gostoso, the distances are greater, between 387 and 875 m. In addition, with the changes in the CL related to the increase in the MSL, such distances will be reduced since the area has an average erosion rate of around 1.2 m/year.

The results show that, in the CVI-USGS (Figure 7A), the medium vulnerability class decreases, while the high vulnerability class increases in proportion as the scenario becomes more pessimistic.

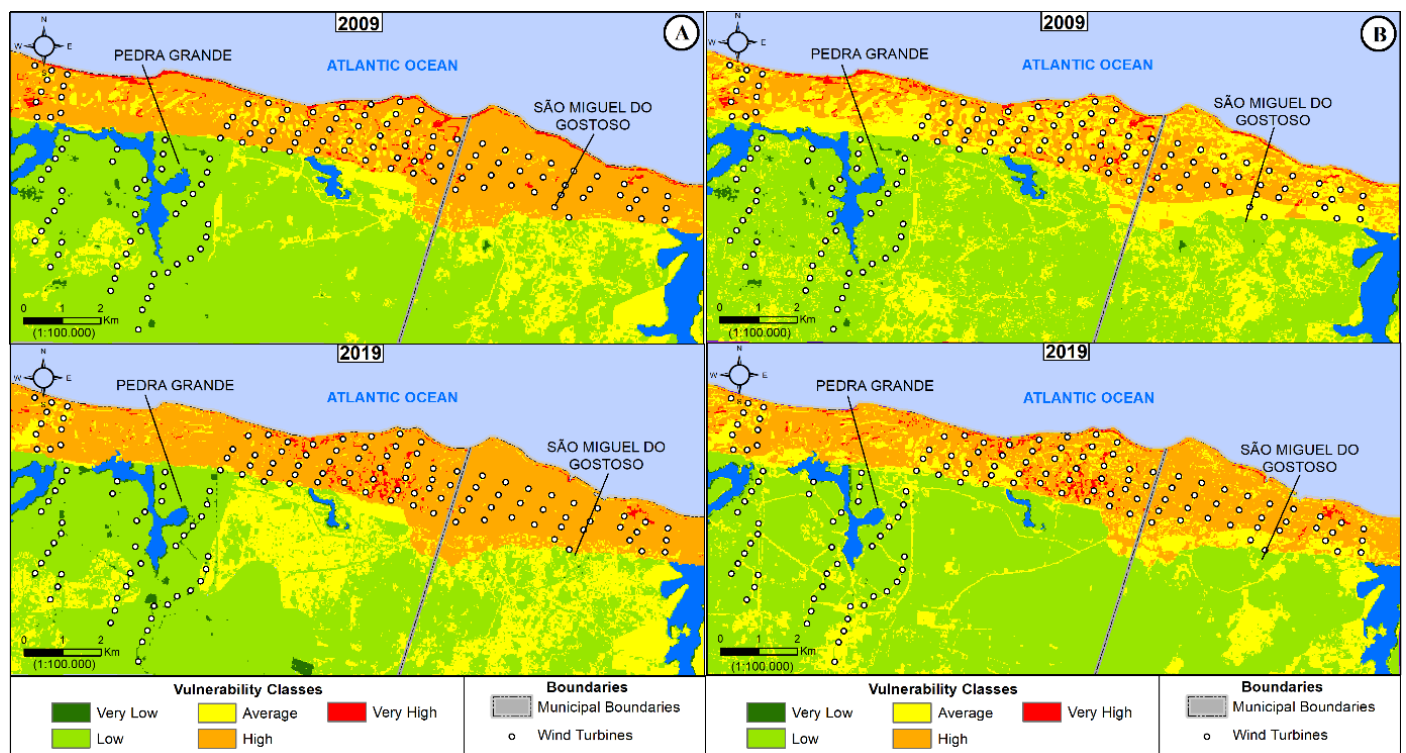


Figure 4 – Map of (A) natural and (B) environmental vulnerability indices of the study area in the years 2009 and 2019 following the hierarchical analytical process.



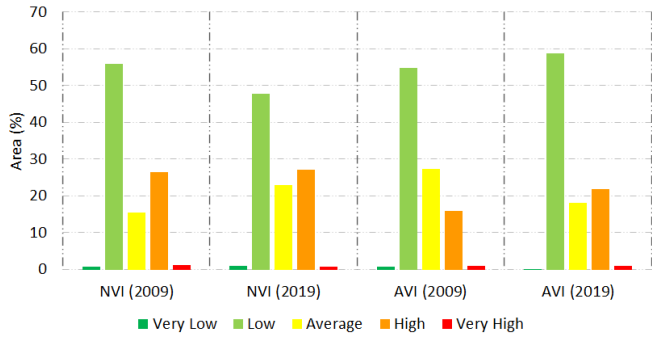


Figure 5 – Percentage in the area of natural and environmental vulnerability indices, weighted through the hierarchical analytical process for the years 2009 and 2019.

Table 4 – Descriptive statistics of coastline variation and prognosis.

Statistics	LRR	NSM	LMS
Mean	-1.18	-37.03	-1.18
Median	-1.04	-32.88	-1.03
Mode	-0.93	-27.23	-1.11
Standard deviation	0.66	21.38	0.67
Variance	0.43	455.92	0.45
Range	3.46	114.64	3.69
Minimum value	-3.14	-103.76	-3.29
Maximum value	0.32	10.88	0.4
Sum	-453.46	-14,218.29	-452.82

LRR: coastline variation rate (m/year); NSM: coastline variation (m); LMS: coastline variation projection for the next 30 years (m/year).

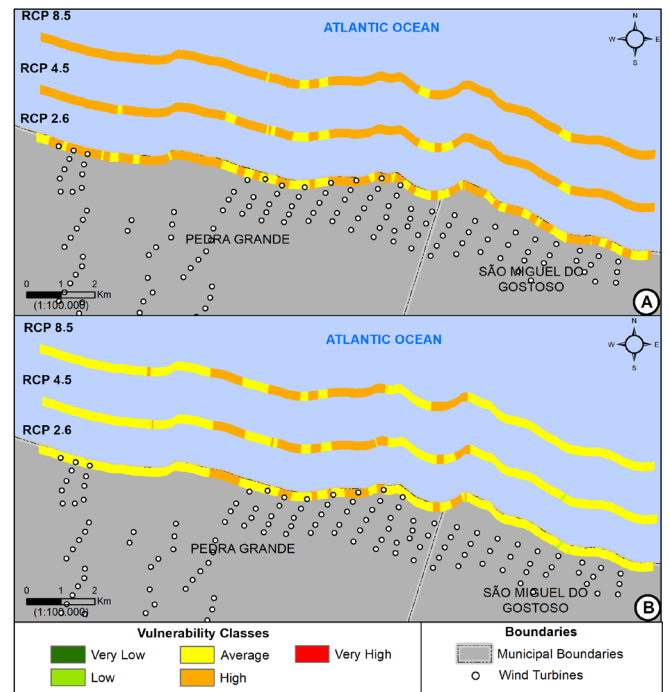


Figure 6 – Maps of the coastal vulnerability indices of the study area in 2019 for the three scenarios of mean sea level variation according to the IPCC (2014), RCP 2.6, RCP 4.5, and RCP 8.5, using the methodology: (A) CVI-USGS and (B) CVI by Busman (2016).

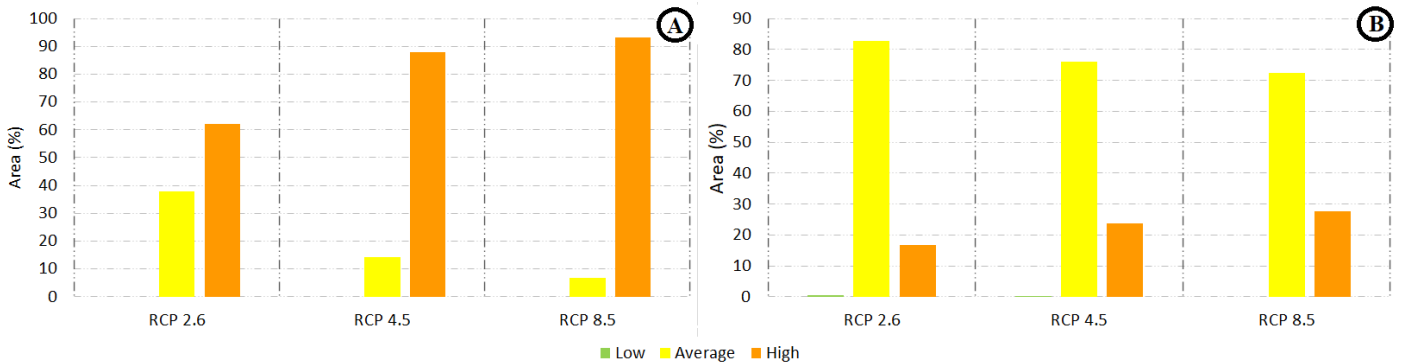


Figure 7 – Percentage in the areas of coastal vulnerability in 2019 for the three scenarios of mean sea level variation according to the IPCC (2014) (RCP 2.6, RCP 4.5, and RCP 8.5) through the methodology: (A) adopted by the USGS and (B) determined by Busman et al. (2016).

For the RCP 2.6 scenario, the proportions were 37.81% for the medium vulnerability class and 62.19% for the high vulnerability class. For the RCP 4.5 scenario, the medium vulnerability class was 14.14% and the high vulnerability class was 87.96%. In the RCP 8.5 scenario, the medium vulnerability class indicated 6.83%, and the high vulnerability class was dominant at 93.17%.

In the CVI methodology (Figure 7B), the low vulnerability class is restricted and barely changes, reaching the value of approximately 0.02% only for RCP 2.6 and RCP 4.5. The medium vulnerability class decreases with the change to a more pessimistic scenario, from 82.85 to 72.46%. In contrast, the proportions of high vulnerability increase from 16.74% in RCP 2.6, reaching 23.84% in RCP 4.5 and 27.54% in RCP 8.5.

However, it should be noted that anthropogenic actions directly on the CL are not the main influencers on the degree of vulnerability, since the addition of these variables in the CVI methodology promoted a reduction in the degree of vulnerability in the investigated scenarios, if compared to the CVI-USGS.

## Conclusion

In this study, thematic maps of geology, geomorphology, pedology, slope, vegetation, and land use and cover were designed for the coastal strip sector between the cities of Pedra Grande and São Miguel do Gostoso. These maps were used as a basis for the creation of the EVI and the NVI for the periods before and after the installation of the União dos Ventos Wind Farm Complex. Similarly, such thematic maps were used to determine the CVIs from the perspective of the following two methods: CVI proposed by Busman et al. (2016) and CVI-USGS. The maps were made at a scale of 1:100,000 with the aid of multispectral and multitemporal images from the LANDSAT satellite for the years 1989, 1999, 2009, and 2019, in addition to field surveys and auxiliary cartographic data from official Federal Government agencies.

The NVI and EVI, in general, had their area proportions assessed in low, medium, high, and very high vulnerability classes. The EVI had the largest variations among the area proportions between the years 2009 and 2019, indicating a strong influence of human action in the local context of the territory. The implementation of the wind farm complex in PPAs contributed to increasing the vulnerability of local ecosystems, especially in sectors with high susceptibility to erosion, such as mobile or fixed dune fields.

According to the observed CVIs, the CL of the region has, for the most part, medium to high vulnerability, with high levels of ero-

sion and low deposition values ranging from 10.88 to -103.76 m. The generated results have the possibility of reaching higher values since these scenarios were estimated and can reach higher rates of MSL increase than expected. The proximity of the wind turbines to the CL makes the evaluation of the CL variation even more relevant since, at certain points, this distance approaches 100 m and can exceed it in a few decades, considering the average erosion rate of 1.2 m/year.

The CVI-USGS showed greater variations between medium and high vulnerability classes for the extension of the CL with changes in the RCP scenarios, since the variables of anthropogenic influence on the CL were only considered for the calculation of the CVI by Busman et al. (2016), which reduces the weight of the other variables present in the equation. The less urbanized area or the area used for any human activity on the CL of the study area contributed to the vulnerability values in the CVI. The low vulnerability class occurs only in restricted sections of the CVI, disappearing in the most pessimistic scenario, which presents the proportions of the high vulnerability class higher than the proportions of the medium vulnerability class. Therefore, the installation of the wind farm complex, represented by the variables of human action, was not the preponderant factor in establishing the degree of vulnerability of the CVI.

The absence of adequate planning and the anticipation of public entities in solving adversities in coastal environments can cause even more serious and costly problems, which makes it valid to recommend the application of studies that formulate indicators, determined with methodologies and variables suitable for different local thematic classes. We also suggest to monitoring the seafront based on high-performance devices in order to monitor local changes in the face of the local effects of global climate change.

## Contribution of authors:

LACERDA, I. L. C.: Conceptualization; Data Curation; Formal Analysis; Methodology; Validation; Writing — Original Draft; Writing — Review & Editing. AMARO, V. E.: Conceptualization; Formal Analysis; Methodology; Supervision; Writing – Original Draft; Writing — Review & Editing. MATOS, M. F. A.: Conceptualization; Formal Analysis; Data Curation; Methodology; Supervision; Writing — Review & Editing. SCUDELARI, A. C.: Conceptualization; Formal Analysis; Methodology; Supervision; Writing — Review & Editing.

## References

- Agência Nacional de Energia Elétrica - ANEEL, 2020. Sistema de Informações de Geração da ANEEL – SIGA (Accessed February, 2020) at: <https://bit.ly/2IGf4Q0>.
- Amaro, V.; Carvalho, R.; Matos, M.; Ingunza, M.; Scudelari, A., 2021a. Avaliação da suscetibilidade do solo à erosão nas falésias do litoral oriental do estado do Rio Grande do Norte. *Revista Brasileira de Geomorfologia*, v. 22, (1), 3-25. <http://doi.org/10.20502/rbg.v22i1.1887>.
- Amaro, V.; Gomes, L.; Lima, F.; Scudelari, A.; Neves, C.; Busman, D.; Santos, A., 2015. Multitemporal Analysis of Coastal Erosion Based on Multisource Satellite Images, Ponta Negra Beach, Natal City, Northeastern Brazil. *Marine Geodesy*, v. 38, (1), 1-25. <https://doi.org/10.1080/01490419.2014.904257>.
- Amaro, V.; Scudelari, A.; Oliveira, D.; Lacerda, I.; Matos, M., 2021b. Análise de Índices de Vulnerabilidade Física com o uso de Geotecnologias na região da Barreira do Inferno/RN. *Revista de Geociências do Nordeste*, v. 7, (2), 179-192. <https://doi.org/10.21680/2447-3359.2021v7n2ID22034>.
- Brasil, 2002. Conselho Nacional do Meio Ambiente – CONAMA. Resolução CONAMA nº 303, de 20 de março de 2002. *Diário Oficial da União*.

- Brasil, 2012. Decreto-lei nº 12.651, de 25 de maio de 2012. Diário Oficial da União.
- Busman, D., 2016. Zoneamento da dinâmica costeira – aplicação de geotecnologias em apoio à gestão costeira integrada na Praia Atalaia-PA e trecho de praias entre os Municípios de Guamaré e Macau-RN, setor sob influência da indústria petrolífera. Doctoral Thesis, Programa de Pós-Graduação em Geodinâmica e Geofísica, Universidade Federal do Rio Grande do Norte, Natal. Retrivied: 2020-18-03, from <https://repositorio.ufrn.br/handle/123456789/21813>.
- Busman, D.; Amaro, V.; Souza Filho, P, 2016. Análise estatística multivariada de métodos de Vulnerabilidade Física em zonas costeiras tropicais. Revista Brasileira de Geomorfologia, v. 17, (3), 499-516. <https://doi.org/10.20502/rbg.v17i3.912>.
- Choudhary, K.; Boori, M.; Kupriyanov, A., 2018. Spatial modelling for natural and environmental vulnerability through remote sensing and GIS in Astrakhan, Russia. Sensing and Space Sciences, v. 21, (2), 139-147. <https://doi.org/10.1016/j.ejrs.2017.05.003>.
- Colton, T., 1974. Statistics in Medicine. New York, Little Brown and Company, 372 pp.
- Crepani, E.; Medeiros, J.; Hernandez, P; Florenzano, T; Duarte, V; Barbosa, C., 2001. Sensoriamento remoto e geoprocessamento aplicado ao zoneamento ecológico-econômico e ao ordenamento territorial. São José dos Campos: INPE, 124 pp.
- Diniz Filho, J.; Diniz, P; Melo, J., 2018. Informes Hidrogeológicos no município de São Miguel do Gostoso/RN. In: XX Congresso Brasileiro de Águas Subterrâneas, Campinas, 2018.
- Diretoria de Hidrografia e Navegação (DHN), 2020. Tábuas de Maré: Porto de Guamaré (Accessed May, 2020) at: <https://www.marinha.mil.br/chm/tabuas-de-mare>
- Empresa Brasileira de Pesquisa Agropecuária (Embrapa), 2018. Sistema Brasileiro de Classificação de Solos. Brasília, Embrapa, 356 pp.
- European Centre for Medium-range Weather Forecasts (ECMWF), 2020. ECMWF Data Server (Accessed November, 2020) at: <https://www.ecmwf.int/>.
- Formigoni, J.; Araújo, A., 2015. Um procedimento para a previsão das alturas e horários das marés nos estuários dos rios Jaboatão e Timbó - RMR / PE. In: XIII Congresso de Iniciação Científica, Recife, 2015.
- Gerrity, B.; Phillips, M.; Chambers, C., 2018. Applying a coastal vulnerability index to san mateo county: implications for shoreline management. Journal of Coastal Research, v. 85, (Suppl. 1), 1406-1410. <https://doi.org/10.2112/SI85-282.1>.
- Gornitz, V., 1991. Vulnerability of the East coast, USA to future sea level rise. Journal of Coastal Research, v. 9, 201-237.
- Gornitz, V.; Daniels, R.; White, T.; Birdwell, K., 1994. The development of a coastal risk assessment database: Vulnerability to sea-level rise in the U.S. southeast. Journal of Coastal Research, (12), 327-338.
- Grigio, A.; Souto, M.; Castro, A.; Amaro, V.; Vital, H.; Diodato, M., 2004. Use of remote sensing and geographical information system in the determination of the natural and environmental vulnerability of the Municipal District of Guamaré, Rio Grande do Norte, Northeast of Brazil. Journal of Coastal Research, v. 39, 1427-1431.
- Hinkel, J.; Nicholls, R.; Tol, R.; Wang, Z.; Hamilton, J.; Boot, G.; Vafeidis, A.; McFadden, L.; Ganopolski, A.; Klein, R., 2013. A global analysis of erosion of sandy beaches and sea-level rise: an application of DIVA. Global and Planetary Change, v. 111, 150-158. <https://doi.org/10.1016/j.gloplacha.2013.09.002>.
- Instituto Nacional de Meteorologia (INMET), 2020. Dados Históricos (Accessed February, 2020) at: <http://www.inmet.gov.br/portal/index.php?r=bdmep/bdmep>.
- Intergovernmental Panel on Climate Change (IPCC), 2014. Fifth Assessment Report. Cambridge, Cambridge University Press.
- Intergovernmental Panel on Climate Change (IPCC), 2019. Sea level rising and implications for low-lying islands, coasts and communities. Cambridge, Cambridge University Press, 126 pp.
- Intergovernmental Panel on Climate Change (IPCC), 2021. Contribution of Working Group I to the Sixth Assessment Report of the Intergovernmental Panel on Climate Change. Cambridge, Cambridge University Press, 3949 pp.
- Koroglu, A.; Ranasinghe, R.; Jiménez, J.; Dastgheib, A., 2019. Comparison of coastal vulnerability index applications for Barcelona Province. Ocean and Coastal Management, v. 178, 104799. <https://doi.org/10.1016/j.ocecoaman.2019.05.001>.
- Liu, D.; Cao, C.; Dubovyk, O.; Tian, R.; Chen, W.; Zhuang, Q.; Zhao, Y.; Menz, G., 2017. Using fuzzy analytic hierarchy process for spatio-temporal analysis of eco-environmental vulnerability chang during 1990-2010 in Sanjiangyuan region, China. Ecological Indicators, Sanjiangyuan, v. 73, 612-625. <https://doi.org/10.1016/j.ecolind.2016.08.031>.
- Loebmann, D.; Maçorano, R.; Silva, G.; Vicente, L.; Victoria, D., 2012. Interpretação de alvos a partir de imagens de satélite de média resolução espacial. Circular Técnica Embrapa, (21), 1-24.
- Luz, C.; Ramos, A.; Silva, G, 2019. Natural and environmental vulnerability of the Jauru River Basin - Mato Grosso state, Brazil. Raega, v. 46, (3), 176-187. <http://doi.org/10.5380/raega.v46i3.67159>.
- Macedo, Y.; Silva, E; Oliveira, V.; Correa Júnior, J. Medeiros, S.; Costa, D.; Cestaro, L, 2017. Serviços ambientais das unidades geoambientais no município de São Miguel do Gostoso/RN, Brasil. Revista de Geografia e Ordenamento do Território, (12), 205-229. <https://doi.org/10.17127/got/2017.12.009>.
- Martínez, C.; López, M.; Winckler, P; Hidalgo, H; Godoy, E.; Agredano, R., 2018. Coastal erosion in central Chile: a new hazard? Ocean & Coastal Management, (156), 141-155. <https://doi.org/10.1016/j.ocecoaman.2017.07.011>.
- Matos, M.; Amaro, V.; Takiyama, L.; Silveira, O., 2011. Estudo sistemático dos processos hidrodinâmicos sazonais de um sistema flúvio-lacustre na região da planície costeira do Amapá, Brasil. Revista Brasileira de Geomorfologia, v. 12, (2), 59-69. <https://doi.org/10.20502/rbg.v12i2.235>.
- Matos, M.; Scudelari, A.; Amaro, V.; Fortes, C., 2017. Integração de modelagem numérica (SWAN) e dados de campo na determinação do clima de ondas no litoral setentrional do Rio Grande do Norte. Revista Brasileira de Geomorfologia, v. 18, (2), 311-328. <https://doi.org/10.20502/rbg.v18i2.1153>.
- Menezes, A.; Pereira, P; Gonçalves, R., 2018. Uso de Geoindicadores para avaliação da vulnerabilidade à erosão costeira através de sistemas de informações geográficas. Revista Brasileira de Geografia Física, v. 11, (1), 276-296. <https://doi.org/10.26848/rbgf.v11.1.p276-296>.
- Nazir, M.; Mahdi, A.; Bilal, M; Sohail, H.; Ali, N.; Iqbal, H., 2019. Environmental impact and pollution-related challenges of renewable wind energy paradigm - A review. Science of the Total Environment, v. 683, 436-444. <https://doi.org/10.1016/j.scitotenv.2019.05.274>.
- Nogueira, L.; Ribeiro, A.; Medeiros, G.; Martins, A.; Longo, R., 2020. Análise integrada dos aspectos e impactos ambientais da atividade operacional em parque eólico no sudoeste da Bahia/Brasil. Revista Gestão & Sustentabilidade Ambiental, v. 9, (4), 40-63. <https://doi.org/10.19177/rgsa.v9e4202040-63>.

- Pantusa, D.; D'Alessandro, F.; Riefolo, L.; Principato, F.; Tomasicchio, G., 2018. Application of a coastal vulnerability index. A case study along the Apulian Coastline, Italy. *Water*, v. 10, (9), 1218. <https://doi.org/10.3390/w10091218>.
- Pereira, B.; Amaro, V.; Silva, D., 2011. Radar and optical hybrid images to improve geoenvironmental mapping in Rio Grande do Norte state, Brazil. *WIT Transactions on Ecology and the Environment*, v. 149, 111-122. <https://doi.org/10.2495/CP110101>.
- Rodrigues, M.; Nepomuceno, A.; Morais, E., 2017. Uma breve descrição do setor de energia eólica no estado do Rio Grande do Norte. Brazil Windpower Conference & Exhibition (Accessed February, 2020) at: <http://abeeolica.org.br/>.
- Saaty, T., 2008. Decision making with the analytic hierarchy process. *International Journal of Services Sciences*, v. 1, (1), 83-98. <https://doi.org/10.1504/IJSSCI.2008.017590>.
- Santos, M.; Amaro, V., 2011. Rede geodésica para o monitoramento costeiro do litoral setentrional do estado do Rio Grande do Norte. *Boletim de Ciências Geodésicas*, v. 17, (4), 571-585. <https://doi.org/10.1590/S1982-21702011000400005>
- Short, A.; Klein, A., 2016. Brazilian beach systems. Coastal Research Library, v. 17, 608 pp.
- Silva, B.; Santos Júnior, O.; Freitas Neto, O.; Scudelari, A., 2020. Erosão em falésias costeiras e movimentos de massa no Rio Grande do Norte, Nordeste do Brasil. *Geociências*, v. 39, (2), 447-461. <https://doi.org/10.5016/geociencias.v39i2.14233>.
- Tricart, J., 1977. *Ecodinâmica*. Rio de Janeiro, IBGE, 91 pp.
- Vieira, I., 2019. Mapeamento da área de preservação permanente na margem norte do Rio Itajaí-Açu em área urbana consolidada. *Metodologias e Aprendizado*, v. 1, 26-29. <https://doi.org/10.21166/metapre.v1i0.641>.